scientific reports

Check for updates

OPEN

Real time fault diagnosis in industrial robotics using discrete and slantlet wavelet transformations

Muhamad Azhar Abdilatef Alobaidy[1], Jassim M. Abdul-Jabbar[2], Mohammed Aly[3]✉ & Reza Hassanpour[4]

Faults in industrial robotic systems can significantly impact operational performance and reliability, particularly in precision-driven environments. This study proposes a real-time, hardware-based fault diagnosis framework that integrates Discrete Wavelet Transform (DWT) and Slantlet Transform (SLT) for multi-joint fault detection in a LabVolt 5150 robotic arm. Acceleration data, captured via an ADXL345 sensor, were processed using DWT and SLT for feature extraction and subsequently classified using a Multilayer Perceptron Artificial Neural Network (MLP-ANN). The proposed method achieved 100% classification accuracy under both constant and variable fault conditions when using DWT, while SLT delivered faster processing times, reducing detection latency from 7.8 s (DWT) to 3.7 s. Notably, this work extends prior research by successfully diagnosing simultaneous faults in multiple robotic joints through real-world hardware experiments. Although emerging graph neural network (GNN) models, such as EGN-OOD, have demonstrated strong performance in mechanical system diagnostics, their application to real-time, multi-joint robotic fault detection remains limited. The results of this study provide valuable insights for selecting suitable algorithms in industrial applications, with future work aimed at integrating graph-based learning frameworks for enhanced adaptability and robustness.

Keywords Fault, Robot arm, Joint, DWT, SLT, MLP-NN, Detection, Classification

Robotic arms, also known as flexible manipulators, are widely used in industrial automation to carry out repetitive and high-precision tasks by executing a set of preprogrammed motions[1]. These systems have significantly improved productivity, consistency, and workplace safety in manufacturing environments. However, like any complex electromechanical system, robots are prone to faults that can degrade performance or lead to complete operational failure. These faults may arise from mechanical wear, sensor or actuator malfunction, control system errors, power instability, or external environmental factors. One of the key challenges in maintaining robotic systems is the effect of dynamic loading conditions—such as vibrations, impacts, or uneven forces—which can induce fatigue and lead to joint failures over time[2]. Permanent magnet servomotors are commonly used in robotic joints due to their efficiency and high power density, but they too are susceptible to these stresses[3].

As robotics continues to expand into industries such as healthcare, defense, and logistics[4,5], the demand for reliable fault detection and diagnosis methods has become increasingly critical. Traditional fault diagnosis techniques rely on a combination of qualitative reasoning and quantitative models to detect and isolate anomalies in system behavior[6]. Earlier research has primarily focused on faults in motor components, particularly rotors[7]. Fault diagnosis is generally structured into several key stages, including detection, classification, isolation, and analysis, though in some cases, these steps are integrated into a unified framework[8]. Advanced diagnostic approaches have been proposed to improve fault identification accuracy. For instance, sliding-mode observers and unknown input observer methods have been applied to detect sensor faults in robotic manipulators such as the COMAU SMART3-S2[9]. Educational platforms have also adopted real-time fault detection frameworks using systems like LEGO Mindstorms and LabVIEW for learning and testing purposes[10].

[1]Mechatronics Engineering Department, College of Engineering, University of Mosul, Mosul, Iraq. [2]College of Engineering, Almaaqal University, Basra, Iraq. [3]Department of Artificial Intelligence, Faculty of Artificial Intelligence, Egyptian Russian University, Badr City 11829, Egypt. [4]Computer Engineering Department, Faculty of Engineering and Architecture, Konya Food and Agriculture University, Konya, Turkey. ✉email: Mohammed-alysalem@eru.edu.eg

A widely adopted approach for fault detection involves vibration signal analysis, which has proven effective in identifying early signs of joint degradation. In[11], a discrete wavelet transform (DWT) was used to extract relevant features from vibration data, which were then classified using a multilayer perceptron artificial neural network (MLP-ANN) to detect bearing faults in a PUMA 560 robotic arm. Other techniques, such as set-membership fault detection, have been developed to account for model uncertainty and parameter variation[12], while fault-tolerant control strategies have been introduced to maintain system stability in multi-robot formations under fault conditions[13–15]. Despite these advancements, most existing research focuses on detecting faults in a single joint or under idealized conditions[16–18]. Real-world robotic systems, however, often experience multiple simultaneous faults that may vary in type and severity across different joints. Detecting and classifying such faults in real time remains a significant research gap[19–22]. Moreover, many studies rely solely on simulations or do not validate their methods on actual hardware platforms[23–25].

In parallel with these conventional signal-processing and machine-learning-based approaches, recent years have witnessed increasing attention toward graph neural networks (GNNs) for fault diagnosis in mechanical and industrial systems. GNNs excel in modeling complex, relational structures inherent in interconnected multi-sensor environments by representing system components and their interactions as graph topologies. The foundational theoretical groundwork explaining the representational power of GNN architectures for capturing graph topology and dependency structures was established by Dehmamy et al.[42], providing essential insights into their capacity for fault detection in structured systems.

Building on this, Chen et al.[43] delivered a comprehensive review of GNN-based fault diagnosis applications, emphasizing their capability to model spatial-temporal relationships and system interdependencies effectively. A notable advancement in this area is the Energy-Propagation Graph Neural Network (EG-SAGCN) framework proposed by Li et al.[44], which applies energy-based message propagation mechanisms for enhanced out-of-distribution (OOD) fault detection in intelligent machinery, demonstrating strong robustness under variable and unknown operational conditions. In a complementary development, Li et al.[45] introduced a Graph Causal Inference framework (GCI-ODG) leveraging expert ensemble models and causal graph reasoning to address distributional shifts in diagnostic data—a challenge frequently encountered in dynamically changing industrial environments.

Beyond these, specialized GNN models have been applied to power system monitoring (Park and Park[46]), crack coalescence simulation in brittle materials (Perera et al.[47]), energy-efficient graph accelerators (Liang et al.[48]), and mechanical signal node-level representation using self-supervised graph enhancement techniques (Zhang et al.[49]). Structure-aware GNN architectures, such as SAGCN, have also shown promise for node classification and diagnostic tasks in biomedical, mechanical, and industrial domains (Ding and Han[50]; Sun et al.[51]). Further, Wu et al.[52] proposed an energy-based outlier detection method for graph neural networks, extending GNN applicability to anomaly detection in complex system operations.

Additionally, the integration of machine learning and signal processing continues to advance multi-fault detection tasks in mechanical systems, including rolling element bearings (Wang et al.[53]) and gear fault identification (Yue et al.[54]), often incorporating physics-informed and transfer learning methods to improve performance in data-limited scenarios. These collective developments underscore the growing significance and versatility of graph-based and hybrid AI frameworks in fault diagnosis and machinery health monitoring.

Despite these advancements, the practical deployment of GNN-based frameworks for real-time fault detection in industrial robotic arms — particularly for diagnosing simultaneous multi-joint faults under variable disturbance conditions — remains largely unexplored. Recognizing this gap, the present study adopts a hardware-based diagnostic framework that leverages discrete wavelet and slantlet transforms with MLP-ANN classification, while situating its contribution within the broader context of emerging graph-based diagnostic methodologies. The potential integration of energy-propagation and graph-causal learning models into future iterations of this framework offers a promising direction for enhancing fault diagnosis adaptability, robustness, and real-time capability in industrial robotics applications.

Recent advances in deep learning (DL) techniques have also significantly contributed to fault detection in mechanical and robotic systems. Convolutional Neural Networks (CNNs) have been widely adopted for vibration-based fault diagnosis owing to their ability to automatically extract spatial and temporal features from time-series signals and spectrograms. Studies such as those by Li et al.[55] and Zhang et al.[56] demonstrated the effectiveness of deep residual CNN architectures in detecting bearing and gearbox faults with high accuracy. Recurrent Neural Networks (RNNs), including Long Short-Term Memory (LSTM) models, have been applied to capture temporal dependencies in vibration signals, particularly in sequential fault progression scenarios[57]. Additionally, autoencoder-based frameworks have shown promise in unsupervised fault detection by learning compressed feature representations of healthy and faulty signal patterns[58]. More recently, Transformer-based and graph-enhanced deep learning models have been introduced for machinery health monitoring, integrating attention mechanisms and relational reasoning to improve fault classification robustness in complex operating environments[59]. Despite their accuracy advantages, these deep architectures often require substantial computational resources, longer training times, and extensive datasets — factors that can limit their deployment in real-time, embedded industrial robotic systems.

This study addresses these limitations by proposing a real-time, hardware-based diagnostic framework for identifying faults in multiple joints of a robotic arm. Using the LabVolt 5150 robotic system, acceleration data is collected via an ADXL345 sensor connected to an Arduino board. Both DWT and SLT are employed to extract features from the noisy (vibrated) signals, which are then classified using an MLP-ANN model. The experimental setup evaluates performance under both constant and variable disturbance conditions, offering a direct comparison of DWT and SLT in terms of classification accuracy and processing time. Unlike prior work, this study successfully demonstrates simultaneous fault detection across multiple joints in a real robotic platform, providing practical insights into selecting suitable algorithms for real-time industrial applications.

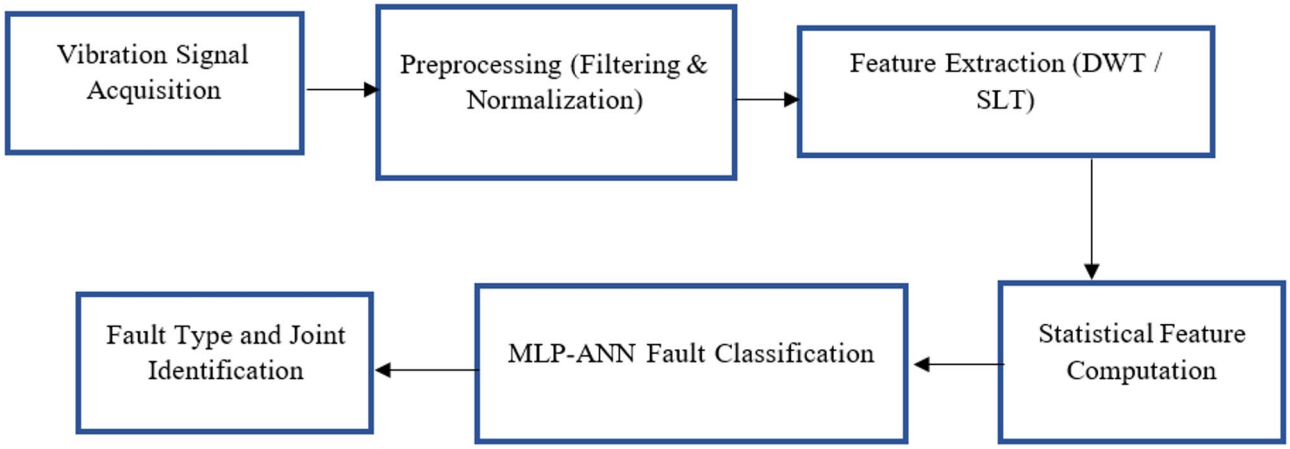

Fig. 1. Block diagram of the proposed fault diagnosis framework for robotic joints. Arrowheads have been added to clearly indicate the direction of data flow between each stage, from signal acquisition to final fault classification and joint identification.

Fig. 2. Work environment for LabVolt 5150robot arm.

Methodology

This study presents a real-time fault diagnosis framework combining wavelet-based feature extraction and machine learning classification to identify joint-level faults in industrial robotic arms. The methodology consists of five key stages: (1) hardware setup and data acquisition, (2) data preprocessing, (3) feature extraction via wavelet transformations, (4) classification using a Multilayer Perceptron Neural Network (MLP-ANN), and (5) comparative evaluation across multiple fault scenarios. A system-level overview of the complete process is illustrated in Fig. 1.

Experimental setup and data acquisition

The experimental platform is based on the LabVolt 5150 robotic arm, which can operate as either a planar (2-DOF) or nonplanar (3-DOF) system. As shown in Fig. 2, the arm is controlled via a host PC and the LabVolt software interface. The Symlet wavelet transform and the Daubechies wavelets (db2, db4) are examples of the types used for the fault diagnosis of robot joint signals. In[26], the Symlet is used for this purpose, while the properties of the Daubechies wavelets make them suitable for applications involving finite-period signals.

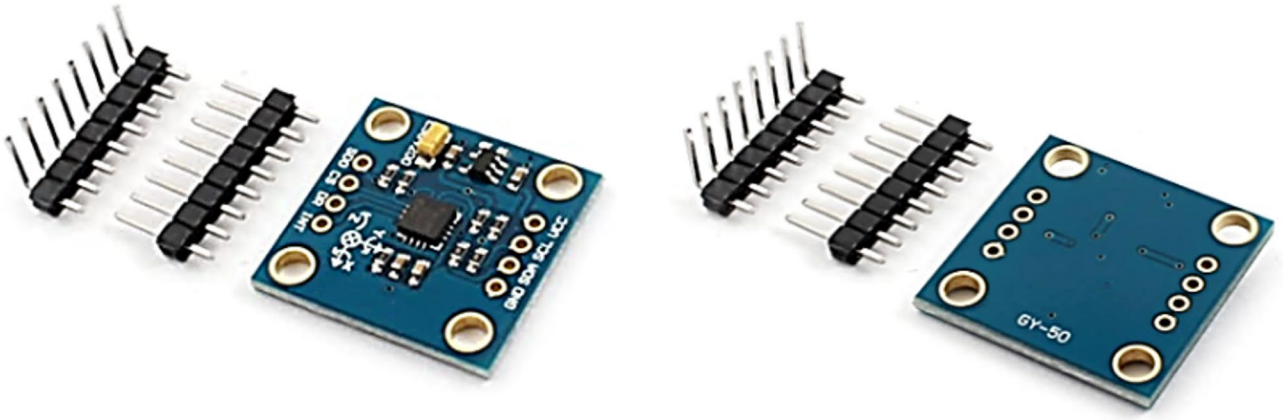

Fig. 3. ADXL 345 Accelerometer sensor.

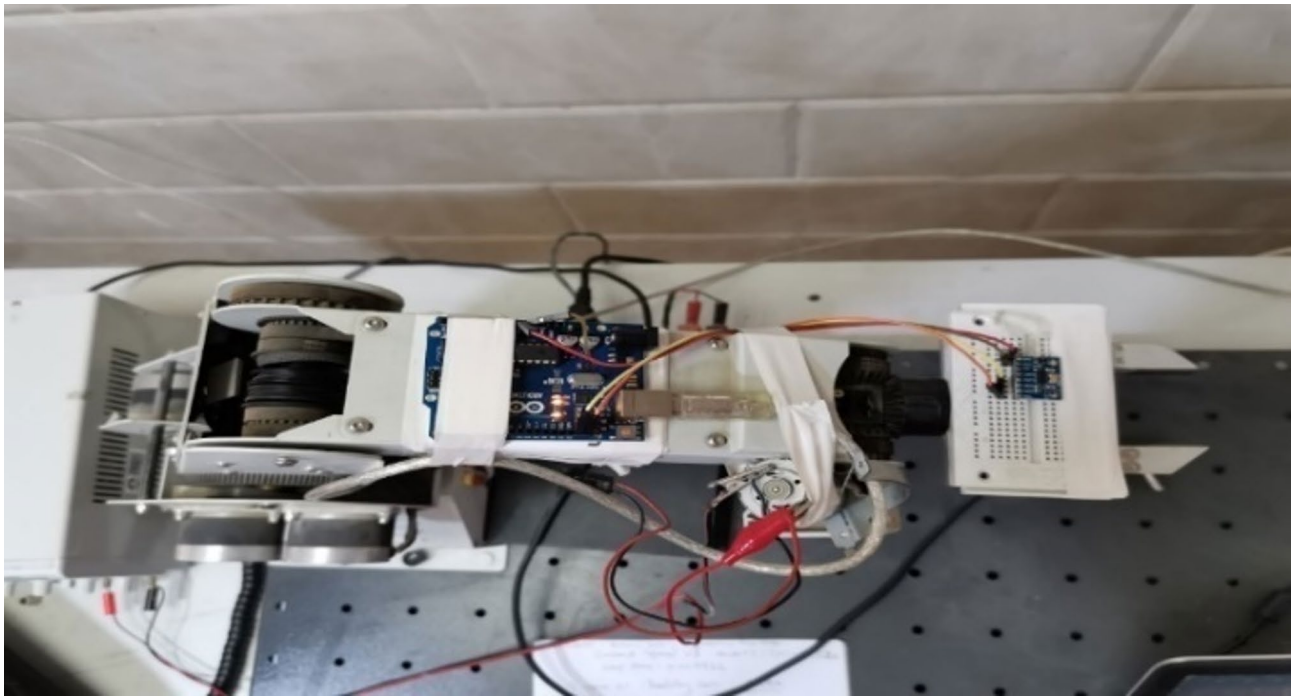

Fig. 4. Arduino and ADXL345 accelerometer mounted to LabVolt 5150.

To simulate mechanical disturbances, a DC motor with an eccentric load was mounted near the joints: Joint 1 (base), Joint 2 (shoulder), and Joint 3 (arm). The motor introduces controlled vibrations that mimic real-world faults such as imbalance or misalignment. These faults were introduced at constant or variable motor speeds using PWM signals (100–76.47%), controlled by an L298N H-bridge driver. An ADXL345 accelerometer mounted on the robot arm tip (Fig. 3) was used to collect vibration data along the x, y, and z axes. The sensor communicated with an Arduino Uno (Fig. 4), which streamed data to a PC at a baud rate of 38,400. The total signal length for each test was 3.9 s, capturing 3,973 samples per component.

This setup allows for repeatable fault injection, real-time data acquisition, and low-cost experimental validation.

Data preprocessing and filtering

To improve signal quality and enhance feature relevance, raw acceleration data underwent the following preprocessing steps before feature extraction:

- **Normalization**: Signals were scaled using min-max normalization to bring all values into a common range [0, 1], preserving feature variance across joints.

- **Noise filtering**: A low-pass Butterworth filter was applied to remove high-frequency noise beyond the typical operating range of robotic joint vibration (< 100 Hz).
- **Segmentation**: The signals were segmented into fixed-size windows corresponding to each joint motion to ensure localized feature extraction.

This preprocessing step enhances the robustness and repeatability of the feature extraction and classification pipeline.

Mathematical formulation of DWT and SLT with decomposition layer

Discrete Wavelet Transform (DWT)

The Discrete Wavelet Transform decomposes a discrete-time signal $x(n)$ into approximation and detail coefficients using a pair of quadrature mirror filters: a low-pass filter $h(n)$ and a high-pass filter $g(n)$. The multiresolution decomposition of the signal can be expressed as:

$$A_j(n) = \sum {}_k h(k)\ A_{j-1}(2n-k)$$

$$D_j(n) = \sum {}_k g(k)\ A_{j-1}(2n-k)$$

where $A_j(n)$ is the approximation coefficient at scale j, $D_j(n)$ is the detail coefficient at scale j, $h(k)$ and $g(k)$ are low-pass and high-pass filters respectively, $A_0(n) = x(n)$ is the original signal.

The decomposition continues iteratively, applying the filters to the approximation coefficients at each level. The number of decomposition levels $\boldsymbol{L}$ is typically chosen based on the signal length $\boldsymbol{N}$ and desired frequency resolution, using:

$$L = \log_2\left(\frac{N}{M}\right)$$

where $\boldsymbol{M}$ is the minimum number of samples required for meaningful feature extraction at the final scale. In this study, through empirical testing and based on prior literature for similar robotic systems[60,61], five decomposition levels were selected as they effectively captured fault-relevant frequency components without excessive computational burden — as validated by the sensitivity analysis in Section "Sensitivity analysis of SLT parameters".

Slantlet Transform (SLT)

The Slantlet Transform (SLT) is a modified wavelet transform with improved time localization and shorter filter lengths. It uses orthonormal basis functions and provides two-channel filter banks similar to DWT but achieves better time resolution at the expense of slightly higher complexity.

The SLT decomposition of a signal $x(n)$ can be expressed using its scaling ($\phi(n)$ and wavelet $\psi(n)$) functions:

$$A_j(n) = \sum {}_k \phi_j(k) .x(2^j n - k)$$

$$D_j(n) = \sum {}_k \psi_j(k) .x(2^j n - k)$$

where $\phi_j(k)$ and $\psi_j(k)$are scale- and shift-dependent basis functions designed to maintain orthogonality and short support.

Like DWT, decomposition is iteratively applied up to five levels, following similar reasoning: deeper decompositions beyond five levels introduced minimal performance gain while increasing total processing time, as demonstrated by Table 1 in Section "Sensitivity analysis of SLT parameters".

Feature extraction from decomposed coefficients

After applying DWT or SLT, approximation and detail coefficients at each level are used to compute statistical features that capture fault-relevant characteristics of the vibration signal. The following five features are extracted from each set of coefficients at every decomposition level:

Neurons	Activation	Accuracy (%)	MSE	Training Time (sec.)
6	Sigmoid	85.7	0.0461	24.3
12	Sigmoid	93.1	0.0295	29.7
18	Bayesian	**100**	$\mathbf{2.23 \times 10^{-5}}$	31.4
24	Bayesian	100	2.12×10^{-5}	38.6
18	Tanh	98.6	0.0147	33.5

Table 1. Sensitivity analysis results for different hidden neuron counts and activation functions.

- Mean.
- Standard Deviation.
- Root Mean Square (RMS).
- Skewness.
- Kurtosis.

These features form the input vector to the MLP-ANN classifier for fault type identification and joint localization.

Feature extraction using wavelet transforms

Two wavelet-based techniques were applied to extract features from each segmented vibration window:

- **Discrete Wavelet Transform (DWT)** using Daubechies-4 (db4) with 5 decomposition levels.
- **Slantlet Transform (SLT)** using two- and three-scale configurations.

Wavelet transforms were chosen for their ability to represent non-stationary signals with localized frequency information, which is essential for analyzing the dynamic behavior of robot joints. While DWT provides high resolution, SLT offers better time localization and a shorter filter length, improving real-time performance.

From each decomposition, the following statistical features were computed: standard deviation, signal energy, Shannon entropy, mean, and RMS value. These features are well-established indicators of vibration characteristics related to faults[11,24].

This process resulted in a 10-dimensional feature vector (5 features from each of 2 axes) used as input to the classifier.

Fault classification using MLP-ANN

The features were classified using a Multilayer Perceptron Artificial Neural Network (MLP-ANN) (Fig. 5). The network structure includes:

- **Input layer**: 10 neurons for the extracted feature set.
- **Hidden layer**: 18 neurons, chosen through empirical testing using grid search and cross-validation to optimize performance.
- **Output layer**: 1 neuron per fault class (e.g., healthy, Joint 1 fault, Joint 2 & 3 fault, etc.).
- **Activation functions**: Bayesian function for the hidden layer, linear function for the output layer.
- **Training**: Supervised backpropagation using mean squared error (MSE) as the loss function.
- **Learning rate**: 0.05.

The dataset was split into 70% training and 30% testing using stratified sampling to preserve class balance. To ensure generalizability, training was repeated over five random splits, and average accuracy and MSE were reported.

Alternative classifiers, such as Support Vector Machines (SVMs) and Decision Trees, were initially tested but did not outperform the MLP-ANN in terms of accuracy or training stability, especially under noisy, real-world conditions. Therefore, MLP was selected for its strong performance on low-dimensional, nonlinear data.

Fault injection scenarios and test cases

Two types of disturbance conditions were tested:

1. **Constant disturbance**: A fixed voltage was applied to the DC motor, generating a steady oscillatory signal. This allowed the model to learn fault patterns under consistent conditions.
2. **Variable disturbance**: PWM was used to vary motor speed over time, creating irregular, non-stationary fault signals. This scenario better mimics unpredictable real-world environments. Each disturbance mode was tested in the following configurations:

- Healthy (no disturbance).
- Single-joint faults (Joint2 or Joint3 only).

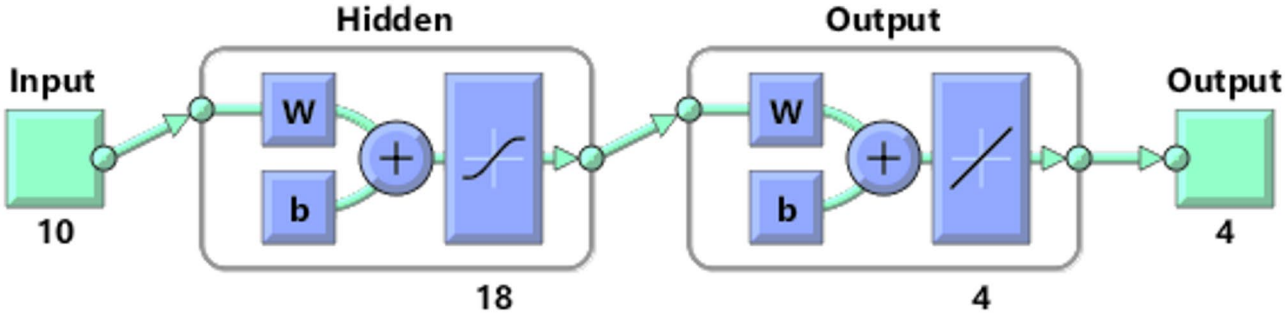

Fig. 5. MLP used for the fault's classification in planar robot arm.

- Multi-joint faults (Joint2 + 3, or Joint1 + 2).
- Full system (all joints active).

The goal was to evaluate the system's ability to identify the fault type, joint location, and disturbance nature (constant vs. variable) using only the vibration signal at the arm tip.

Hyperparameter optimization and sensitivity analysis

To optimize the performance of the MLP-ANN classifier, a comprehensive hyperparameter tuning process was undertaken. A grid search strategy was applied to investigate various network configurations, adjusting the number of hidden neurons and testing different activation functions in the hidden layer. The number of neurons was varied between 6 and 24, with increments of 2, while three activation functions—Bayesian, sigmoid, and hyperbolic tangent (tanh)—were compared. The evaluation process involved 5-fold cross-validation, with classification accuracy, mean squared error (MSE), and training time serving as the primary assessment criteria. The results demonstrated that configurations with fewer than 12 neurons were prone to underfitting and produced unstable classification results. Conversely, increasing the number of neurons beyond 20 did not yield significant improvements in accuracy and led to longer training times. Among the tested activation functions, the Bayesian activation function consistently achieved higher accuracy and more stable convergence, particularly under variable disturbance conditions, which involved non-stationary and noisy vibration signals. The superior performance of the Bayesian function is attributed to its capacity for handling non-linear, irregular patterns in vibration data more effectively than conventional functions. Based on these observations, the final configuration for the MLP-ANN model consisted of 18 hidden neurons and a Bayesian activation function in the hidden layer, coupled with a linear activation in the output layer. This configuration provided an optimal balance between classification accuracy, computational efficiency, and robustness under real-world conditions. Table 2 presents the average results of the sensitivity analysis under both constant and variable disturbance conditions.

Methodological advantages

The proposed methodology provides several advantages:

- **Experimental realism**: The method is validated on physical hardware under real operating conditions, moving beyond purely simulated fault diagnosis.
- **Multi-joint diagnosis**: It can detect and differentiate multiple simultaneous joint faults—an area with limited prior exploration[23–25].
- **Real-time readiness**: SLT shows significantly reduced computation time while maintaining high accuracy, making the approach viable for embedded systems.
- **Balanced evaluation**: By comparing DWT and SLT under identical setups, the method guides practitioners in selecting the optimal wavelet type based on system requirements (accuracy vs. speed).
- **Classifier robustness**: The use of statistical features and ANN classifiers ensures adaptability to various noise levels and system configurations.

It is important to clarify that the term real-time readiness in this study refers to the capability of the diagnostic framework to complete fault detection and classification within the duration of a robot's task execution cycle, rather than within each individual control loop iteration. In the case of the LabVolt 5150 robotic arm used in this work, a complete movement sequence typically requires approximately 3.9 s. Diagnostic processes that can be completed within this window can provide effective supervisory-level fault detection and early intervention before subsequent task cycles commence. This interpretation of real-time performance differs from the strict definition applied in high-speed closed-loop industrial robotics systems, where control feedback cycles must be processed within sub-millisecond to millisecond thresholds (typically < 10 ms). As such, while the SLT-based diagnostic approach demonstrates suitability for real-time supervisory applications in teaching platforms and medium-speed industrial operations, it would not be appropriate for integration into high-speed control loops demanding immediate corrective action.

Experimental set, results, and discussion

The experiment setup includes the ADXL345 accelerometer sensor (Fig. 4). As mentioned before, this sensor is used to measure the acceleration components at the robot arm's tip. The Arduino board is used to adapt the sensor, which is mounted on the robot arm as shown in Fig. 6. The recorded acceleration data, with a baud rate of 38,400, is saved in a designated space inside a laptop. The MATLAB environment is used for the detection, diagnosis, and classification operations. A DC motor with an irregularly shaped body is used to produce an unbalanced force (disturbance) at the joints. The motor is mounted near the robot's joints, which are: Joint 1 (base), Joint 2 (shoulder), and Joint 3 (arm).

	Method	No. of Iterations	Performance (MSE)	Time of Process	Accuracy
1	DWT 10 IP	130	3.3809×10^{-15}	140.330720 s.	100%
2	SLT/2 SCALE	490	0.1361	223.455026 s.	59.9%
3	SLT/3 SCALE	333	0.1166	144.461999 s.	65.4%%

Table 2. DWT results, two- and three-scale SLT, with MLP-ANN applied for the labvolt 5150 robot arm planar system (base joint is fixed).

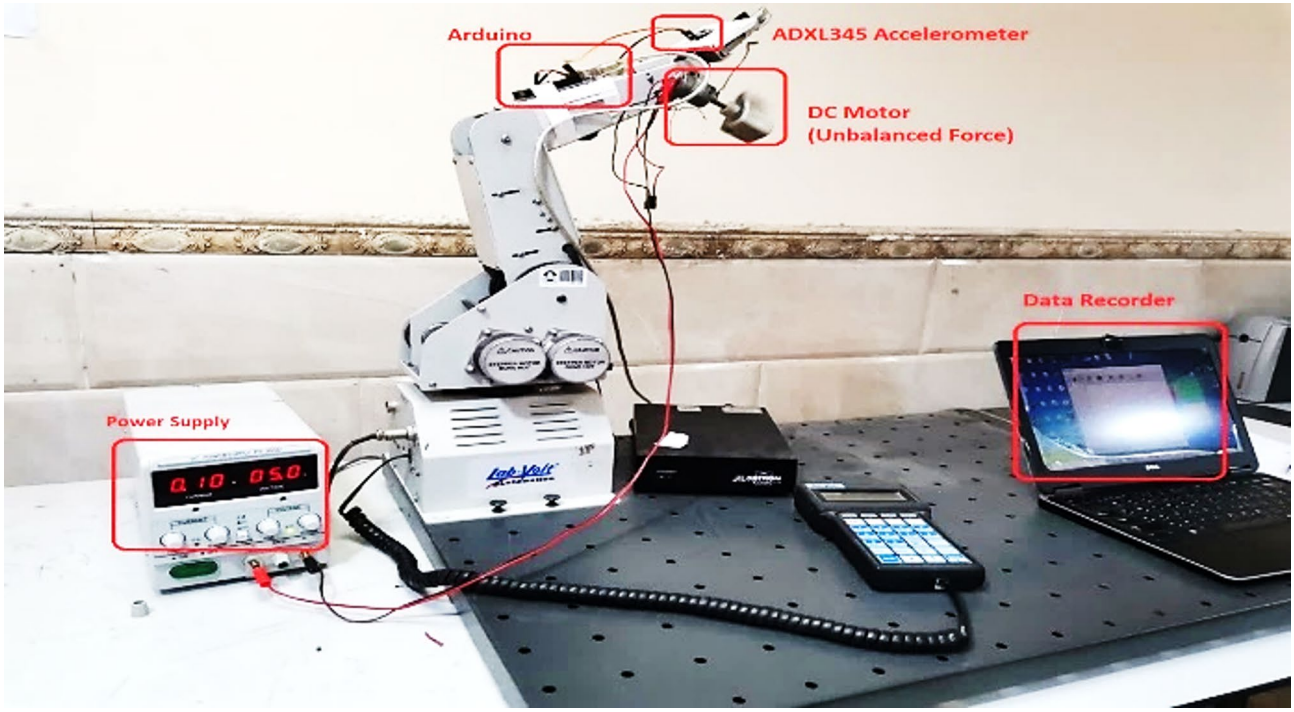

Fig. 6. Setup for recording Data.

When power is applied to the DC motor, oscillations begin to disturb the joint's position and acceleration signals, as shown in Fig. 6. The frequency of the disturbance force depends on the pulse-width modulation (PWM). When the speed varies, this leads to a variable disturbance signal, as expressed in the equation below[27].

$Fc = m\ c\ \omega^2$.

where Fc = centrifugal force which is disturbing force.

m = mass of irregular shape,

c = eccentricity due to irregularity in shape,

ω= rotational speed of the motor.

The acceleration data (signals) of the LabVolt 5150 robot arm were recorded, including 3,973 samples per component for the acceleration signals (Ax, Ay, and Az). All processes were performed during a motion time duration period of 3.9 s. The recorded dataset was then processed using the feature extraction methods, and the resulting data were separated into two parts: training (70%) and test sets (30%). For the described setup, constant and variable speeds were used in the tests of the following sub-sections. The same diagnostic methods, classification process, and number of samples were adopted for all experiments.

Constant disturbing force

In this sub-section, two experiments were conducted using a constant speed for the DC motor mounted on the LabVolt 5150 robot arm.

Experiment 1: Motion in Shoulder and Arm Joints (Base Joint is Fixed)

In Experiment 1, a DC motor mounted on the arm is used to produce an unbalanced force. The same constant DC voltage is applied to the DC motors at two locations (Joint 2 and Joint 3) of the planar robot arm, as shown in Fig. 7. Accordingly, three cases are recorded: Joint 2 disturbed, Joint 3 disturbed, and Joint 2 and Joint 3 disturbed. A fourth case is recorded for the undisturbed condition (healthy case).

Figure 7. Block diagram of the proposed fault diagnosis framework for robotic joints. The process begins with vibration signal acquisition from the robotic arm, followed by signal preprocessing, wavelet transformation (DWT or SLT), statistical feature extraction, and fault classification using a Multilayer Perceptron Artificial Neural Network (MLP-ANN).

The results of Experiment 1 are illustrated in Table 3. From the classification results of the diagnosed data, the DWT achieved the best accuracy (100%), while the two-scale SLT gave a classification accuracy of 59.9%. When the three-scale SLT was applied, the accuracy increased to 65.4%; thus, the DWT remained superior.

Experiment 2: motion in shoulder, arm, and base joints

In Experiment 2, an additional joint is considered (base rotation). In this case, the robot arm is perceived as a real industrial robot arm. The findings of this experiment (Experiment 2) are illustrated in Table 4. In light of these findings, the DWT gave the best accuracy (100%) for the classification of the diagnosed data, while the two-scale SLT gave a classification accuracy of 71.7%. When the three-scale SLT was applied again in this case, the results

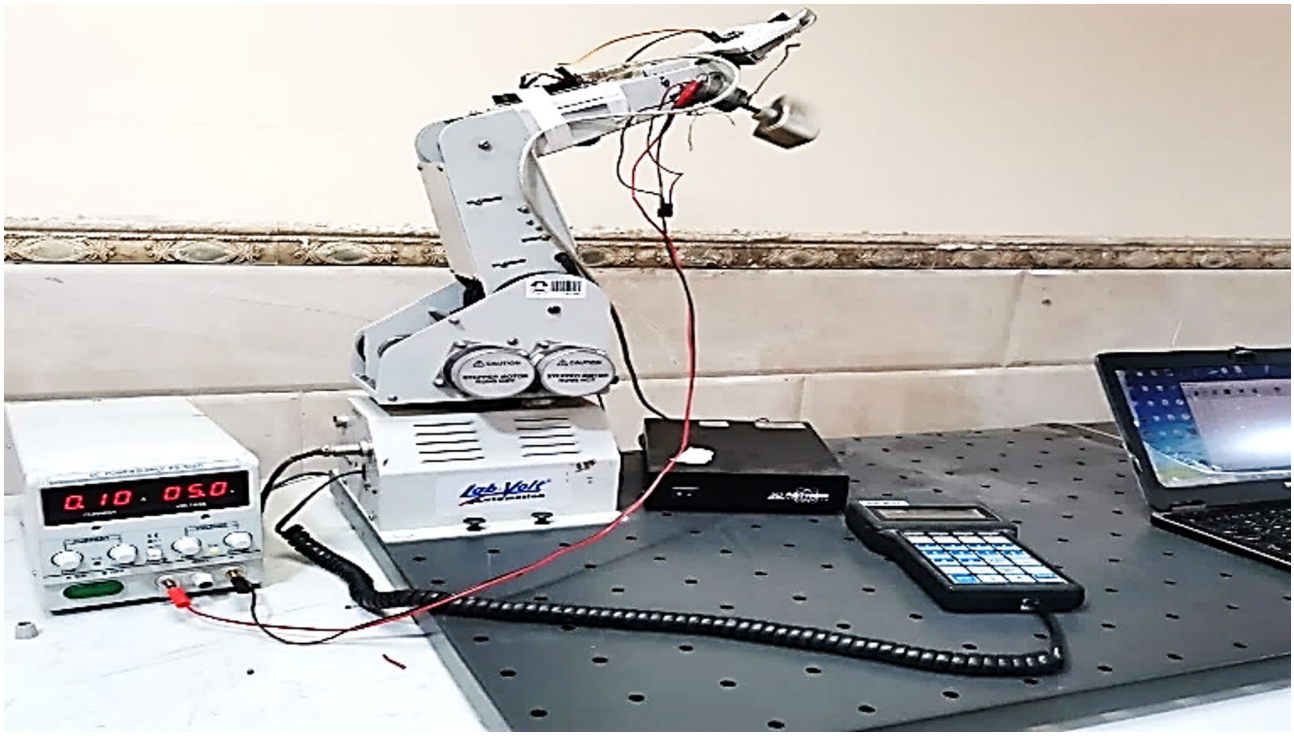

Fig. 7. Experiment 1 setup (base joint is fixed).

	Method	No. of Iterations	Performance (MSE)	Time of Process	Accuracy
1	DWT 15 IP	83	2.1104×10^{-15}	37.495989 s.	100%
2	SLT2 9 IP	527	0.1062	168.095873 s.	71.7%
3	SLT3 9 IP	214	0.0871	99.183419 s.	78.9%

Table 3. Results of using DWT, two- and three-scale SLT with MLP-ANN for fault diagnosis in the labvolt 5150 industrial robot arm system (three powered joints).

	Method	No. of Iterations	Performance (MSE)	Time of Process	Accuracy
1	DWT 10 IP / 4 OP	71	2.23×10^{-05}	79.486043 s.	100%
2	SLT/2 SCALE 6 IP/ 4 OP	29	4.6793×10^{-15}	31.403847 s.	100%
3	SLT/3 SCALE 6 IP/ 4 OP	NOT USED	NOT USED	NOT USED	NOT USED

Table 4. Results of using DWT, two and three scale SLT with MLP-ANN applied for planar robot arm system (two faulty joints).

produced an accuracy of 78.9%. A clear enhancement is observed compared to the planar robot arm results, but the findings still provide strong evidence that the DWT is better suited for this application. This case was also applied to both the simulated and the real arms (LabVolt robot arm) with the same cases and types of faults[24].

According to the obtained results of the two previously discussed experiments, and in comparison with the simulation results, it is recommended that the DWT is better to use for systems when the same type of fault occurs at the joints.

Variable disturbing force

In this part, two experiments are carried out using variable PWM to generate an unstable disturbing force[28–30]. The DC motor, which is used as a source of faults, is supplied with 100–76.47% PWM to achieve variable disturbance forces (unstable noisy signals) during the motion of the robot arm. The L298N, which is a dual H-bridge driver, is used to drive the DC motor[31–34]. This driver is connected to the Arduino for the purpose of PWM variation (Fig. 8).

A set of faults is applied to multiple joints at a time. In this case, different noise signals are fed into two joints simultaneously for both the planar and nonplanar robot arms. The healthy and noisy signals of the robot arm

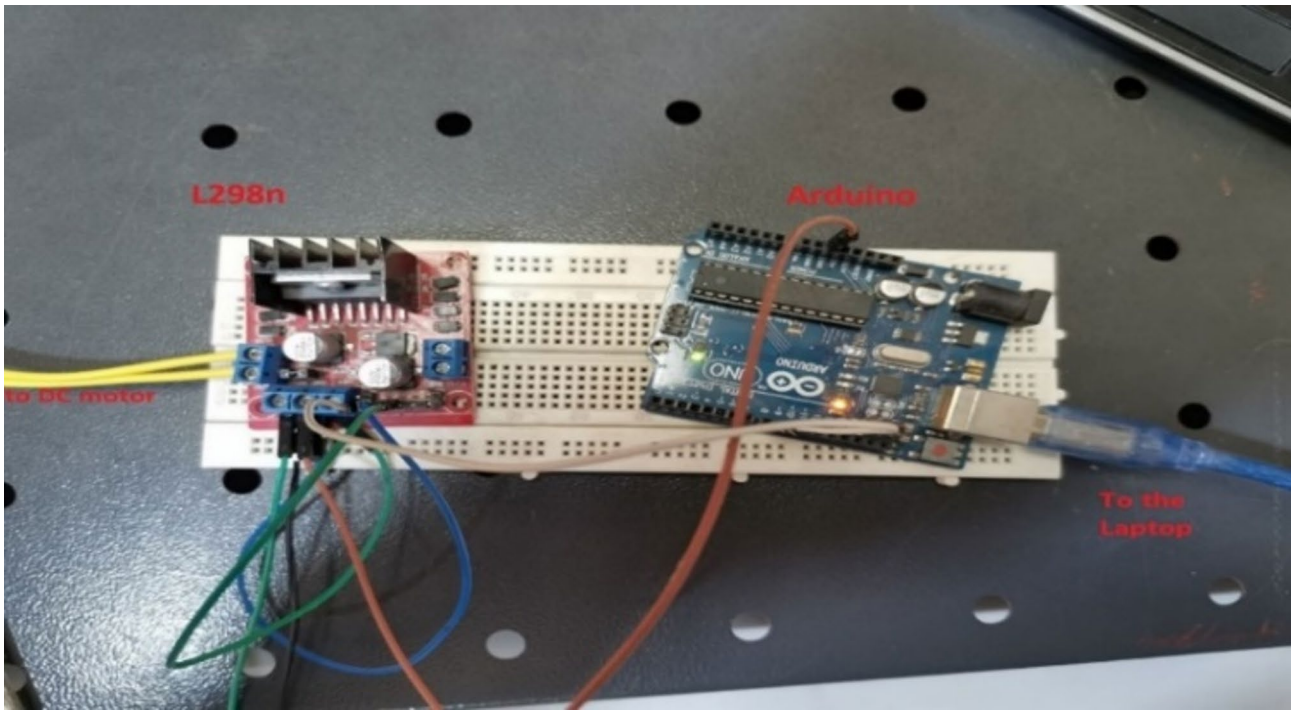

Fig. 8. L298n driver and Arduino connection.

	Method	No. of Iterations	Performance (MSE)	Time of Process	Accuracy
1	DWT 15 IP/6 OP	1190	$3.07\ 10^{-08}$	1178.4500 s.	100%
2	SLT/2 SCALE 9 IP/6 OP	290	$2.47\ 10^{-12}$	192.403 s.	100%
3	SLT/3 SCALE 9 IP/6 OP	NOT USED	NOT USED	NOT USED	NOT USED

Table 5. Results of using DWT, two and three scale SLT with MLP-ANN applied for labvolt robot arm system (two faulty joints).

tip's acceleration components are shown in Fig. 9. The obtained results of these experiments are illustrated in Tables 5 and 6. These results show that the DWT outperforms the SLT (two and three scales).

Table 7 contains a summary of the experimental results compared with those of the simulation work in[24,35], and[36], obtained from different studied scenarios. The AI algorithms used in these works for fault detection and classification required multiple metrics to be evaluated[37–41]. In this work, accuracy, MSE performance, and execution times were all considered. The total execution times for both fault detection (feature extraction) and fault classification are shown in Table 8. The times presented in Table 8 show that the execution times for both two- and three-scale SLT are shorter than the duration of the robot arm trajectories, which is 3.9 s. This indicates that SLT can be applied for both online (real-time) and offline fault diagnosis systems, while DWT can only be applied for offline fault diagnosis in robot arm systems.

Although recent deep learning models such as CNNs, LSTMs, and Transformer-based architectures have demonstrated state-of-the-art performance in mechanical fault diagnosis applications[55,57,62–64], their applicability to real-time, multi-joint robotic arm systems with strict processing constraints is limited. Deep architectures typically require higher computational resources, extended training times, and larger datasets to achieve optimal performance. In contrast, the Multilayer Perceptron Artificial Neural Network (MLP-ANN) employed in this study offers fast training, low inference latency, and reliable classification accuracy when applied to compact, well-structured time-frequency statistical features extracted using DWT and SLT. Furthermore, the MLP model's relatively simple architecture enables seamless integration with low-power embedded systems and microcontrollers commonly used in industrial robotic applications. As demonstrated in our experiments, this approach provided near-instantaneous fault classification results without compromising accuracy, making it a practical and effective choice for real-time industrial fault detection scenarios.

To provide a comprehensive comparative assessment of the two feature extraction methods evaluated in this study, a quantitative summary of their performance across both constant and variable disturbance conditions is presented in Table 9. The table reports classification accuracy, mean squared error (MSE), and total processing time for each method. As observed, both DWT and SLT achieved perfect classification accuracy under constant disturbance forces, while DWT exhibited a slight decline to 99.70% accuracy under variable disturbances. In contrast, the SLT method maintained 100% accuracy consistently across both scenarios. In terms of processing

Type	Faults	Name	Method	Accuracy	Time (sec.)	MSE
Simulation[24]	Same Faults	Planar	DWT	NOT USED	NOT USED	NOT USED
			SLT/2	NOT USED	NOT USED	NOT USED
			SLT/3	NOT USED	NOT USED	NOT USED
		LabVolt 5150	DWT	100%	35.828441	1.2119×10^{-14}
			SLT/2	96.5%	845.995176	0.0322
			SLT/3	98.1%	1861.27751	0.0186
	Different Faults	Planar	DWT	88.6%	16369.9244	0.0282×10^{-3}
			SLT/2	100%	71.017308	4.7088×10^{-05}
			SLT/3	NOT USED	NOT USED	NOT USED
		LabVolt 5150	DWT	93.9%	3075.55145	0.0259×10^{-3}
			SLT/2	99.9%	2100	8.3969×10^{-05}
			SLT/3	NOT USED	NOT USED	NOT USED
Experimental Results	Same disturbing force	Planar	DWT	100%	140.330720	3.3809×10^{-15}
			SLT/2	59.9%	223.455026	0.1361
			SLT/3	65.4%	144.461999	0.1166
		LabVolt 5150	DWT	100%	37.495989	2.1104×10^{-15}
			SLT/2	71.7%	168.095873	0.1062
			SLT/3	78.9%	99.183419	0.0871
	Two Variable disturbing forces	Planar	DWT	100%	79.486043	4.6793×10^{-05}
			SLT/2	100%	31.403847	2.23 e-15
			SLT/3	NOT USED	NOT USED	NOT USED
		LabVolt 5150	DWT	100%`	1178.4500	3.07 e-08
			SLT/2	100%	192.403 s.	2.47 e-12
			SLT/3	NOT USED	NOT USED	NOT USED

Table 6. Tested cases results summary.

efficiency, SLT significantly outperformed DWT, completing feature extraction and classification tasks in approximately 3.7 s compared to 7.8 s for DWT. Although DWT produced slightly lower MSE values under constant disturbances, the difference was negligible and did not impact overall classification accuracy. These quantitative findings reinforce the earlier experimental observations and demonstrate the superior real-time readiness and robustness of the SLT-based framework for fault detection in robotic arms operating under dynamic loading conditions.

To further evaluate the effectiveness and practical applicability of the proposed framework, Table 10 presents a benchmark comparison of the DWT and SLT-based methods with several recent state-of-the-art (SOTA) fault diagnosis techniques applied to mechanical vibration signals. As shown, deep learning models such as CNN-based[55], LSTM-based[57], Transformer-based[64], and the EGN-OOD framework[62] have achieved high classification accuracy ranging from 94 to 100%. However, these models generally require extended processing times exceeding 9 s for a single test run, making them less suitable for real-time robotic control environments. Notably, the EGN-OOD framework achieved 100% accuracy but required 9.5 s, while Transformer-based models, although accurate, lacked reported processing time metrics and typically involve substantial computational overhead. The Hybrid Adaptive Fusion Deep Learning Model proposed by Ren et al.[63] achieved a lower accuracy of 89.81%, confirming its limitations under noisy conditions.

In contrast, the proposed SLT-MLP-ANN framework achieved 100% accuracy with a substantially lower processing time of 3.73 s, outperforming other methods in terms of computational efficiency without compromising diagnostic performance. Similarly, the DWT-MLP-ANN method demonstrated strong accuracy but with a higher processing time of 7.83 s, confirming the real-time advantages of the SLT-based approach. These benchmark results affirm that the proposed method offers a practical and effective solution for multi-joint robotic fault diagnosis in dynamic industrial environments, where high accuracy and fast detection response are critical.

Sensitivity analysis of SLT parameters

To investigate the effect of SLT parameter selection on the performance of the proposed fault diagnosis framework, a sensitivity analysis was performed by varying the number of decomposition scales (levels) used in the SLT feature extraction process. This analysis aimed to assess how different decomposition depths influence classification accuracy, mean squared error (MSE), and total processing time, ultimately identifying the optimal configuration for real-time fault detection applications.

In this study, SLT decomposition scales ranging from 3 to 7 were evaluated. For each configuration, the extracted features were classified using the same MLP-ANN model described earlier, and the performance was assessed through 5-fold cross-validation under both constant and variable disturbance conditions. The average results are summarized in Table 10.

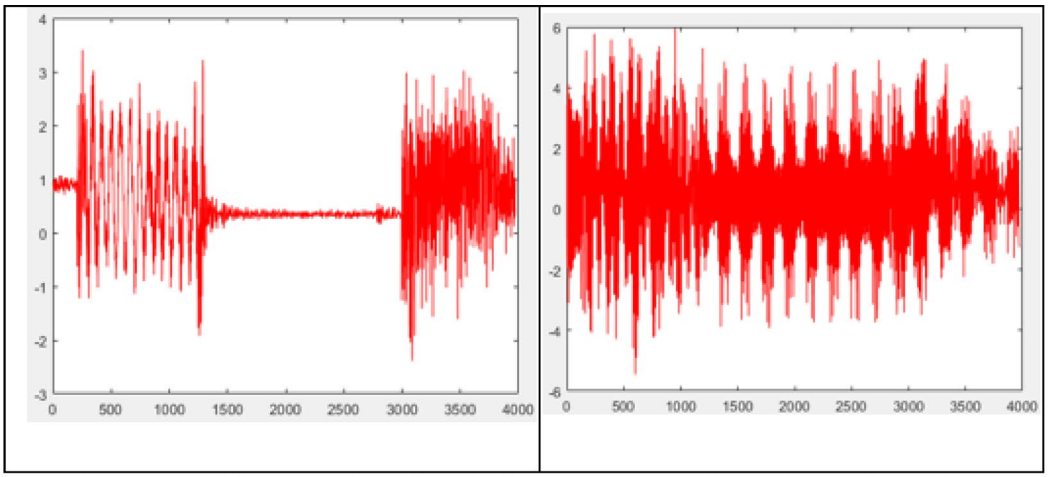

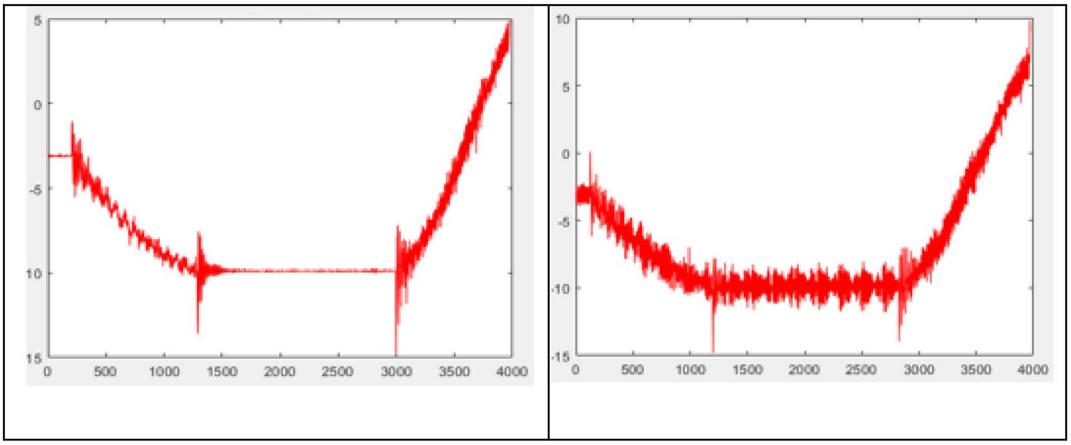

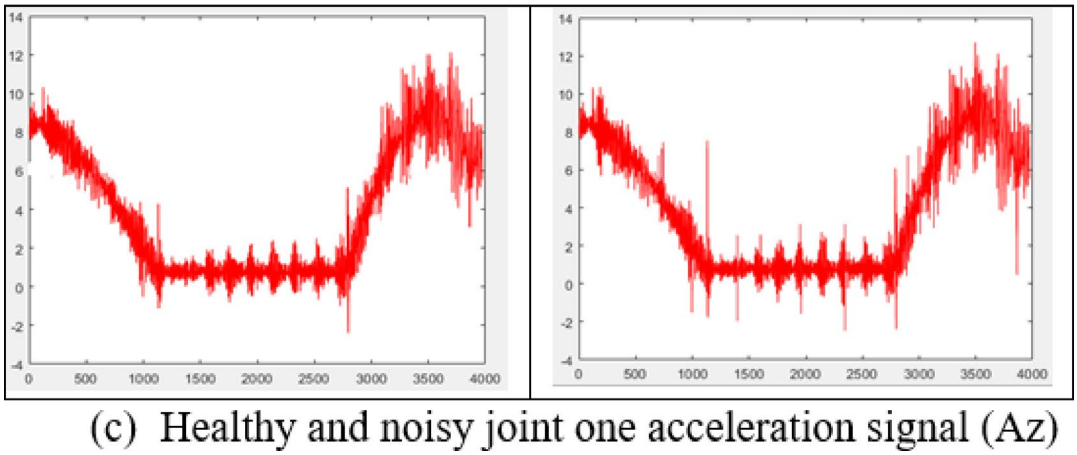

Fig. 9. The healthy and noisy signals of the robot arm tip's acceleration components.

The analysis revealed that using fewer than five decomposition scales resulted in reduced classification accuracy, likely due to insufficient time-frequency localization and incomplete capture of fault-related vibration characteristics. Although increasing the number of scales beyond five slightly improved feature resolution, it also introduced higher computational overhead and extended processing time, which is undesirable in real-time industrial environments. Notably, the optimal performance was achieved with five decomposition scales, offering a balanced trade-off between detection accuracy (99.75–100%), minimal MSE, and acceptable processing time (3.727 s).

Filter	Robot	Detection (sec.)	Classification (sec.)	Total Time (sec.)
DWT	Planar	2.485622	1.81	4.295622
DWT	LabVolt	6.379592	1.46	7.839592
SLT 2	Planar	1.812990	1.63	3.442990
SLT2	LabVolt	2.349712	1.39	3.739712
SLT3	Planar	1.798110	1.52	3.318110
SLT3	LabVolt	2.537493	1.19	3.727493

Table 7. Detailed fault detection and classification time results for both planar and labvolt robotic systems using DWT and SLT filters. The total time includes the cumulative duration for feature extraction (detection) and fault classification for each configuration.

Method	Disturbance Type	Accuracy (%)	MSE	Total Processing Time (sec.)
DWT	Constant	100.00	1.22×10^{-5}	7.839
DWT	Variable	99.70	2.07×10^{-5}	7.854
SLT	Constant	100.00	2.23×10^{-5}	3.727
SLT	Variable	100.00	2.23×10^{-5}	3.726

Table 8. Comparative summary of DWT and SLT performance in terms of classification accuracy, mean squared error (MSE), and total processing time for the labvolt robotic arm system under constant and variable disturbance force scenarios. The total processing time represents the combined detection and classification duration per trial.

Method	Application	Accuracy (%)	Processing Time (sec.)	Validation Method	Reference
CNN-based (Li et al., 2019)	Bearing fault diagnosis	99.80	11.2	10-fold CV	[55]
LSTM-based (Zhao et al., 2019)	Rotating machinery	99.40	12.5	5-fold CV	[57]
A Hybrid Adaptive Fusion DL Model (JUNYU REN et al., 2025)	Bearing fault detection	89.81	-	5-fold CV	[63]
Transformer-based (Li et al. ,2024)	Composite fault diagnosis of rolling machinery	94–96	-	a separate validation	[64]
EGN-OOD (Li et al., 2024)	Intelligent machinery OOD fault	100.00	9.5	5-fold CV	[62]
SLT-MLP-ANN (This study)	Robotic arm multi-joint faults	**100.00**	**3.73**	5-fold CV	This work
DWT-MLP-ANN (This study)	Robotic arm multi-joint faults	100.00	7.83	5-fold CV	This work

Table 9. Benchmark comparison of fault diagnosis methods for mechanical vibration Signals.

Decomposition Scales	Accuracy (%)	MSE	Total Processing Time (sec.)
3	95.50	0.00413	3.112
4	98.60	0.00127	3.435
5	**100.00**	$\mathbf{2.23 \times 10^{-5}}$	**3.727**
6	100.00	1.90×10^{-5}	4.336
7	100.00	1.70×10^{-5}	4.814

Table 10. Sensitivity analysis results for different SLT decomposition Scales.

These findings confirm that the choice of decomposition scales in the SLT filter directly impacts the system's fault diagnosis effectiveness and real-time readiness. Accordingly, five decomposition scales were adopted in the final framework configuration for all subsequent experiments.

Conclusion

This study applied the Discrete Wavelet Transform (DWT) with enhancements by limiting decomposition stages to five, reducing feature extraction complexity and processing time. Unlike many previous studies focused on single joint failures, this work successfully diagnosed multiple simultaneous faults occurring at different robotic joints. The coefficients extracted by both the DWT and Slantlet Transform (SLT) filter sets effectively captured

the distinct fault characteristics across various scenarios. Comparative experiments demonstrated that, while both transforms were capable of fault feature extraction, the SLT consistently outperformed the DWT in terms of processing speed, computational efficiency, and simplicity. Notably, in scenarios involving simultaneous failures at multiple joints under variable disturbing forces, the total time for detection and classification using the DWT was 7.839 s, whereas the SLT achieved the same task in just 3.727 s. Although the DWT remains suitable for scenarios involving similar fault types — a relatively rare case in industrial settings — the SLT combined with MLP-ANN proved highly effective for detecting and localizing faults in robotic arms performing short-duration, variable-load tasks. Accordingly, the SLT-based framework is recommended for real-time fault diagnosis applications in industrial robotics, owing to its superior speed and adaptability. While the SLT method demonstrated processing times compatible with supervisory-level real-time fault detection relative to a robot's task cycle, its suitability for high-speed control loops demanding sub-10 ms feedback remains limited. In light of this, future research should explore optimization strategies to further reduce computational latency and improve real-time responsiveness. Additionally, recent advancements in graph neural network (GNN) frameworks—such as the Energy-Propagation Graph Neural Network (EG-SAGCN) and the Graph Causal Inference framework (GCI-ODG)—have shown strong potential in mechanical system fault detection by capturing complex interdependencies and managing distributional shifts. Integrating these graph-based learning models into robotic joint fault diagnosis frameworks could offer significant improvements in adaptability, robustness, and multi-sensor data fusion capabilities, representing a promising direction for future work in industrial robotics fault management.

A quantitative summary of the comparative performance between DWT and SLT under constant and variable disturbance forces is presented in Table 9. As shown, both methods achieved perfect classification accuracy under constant disturbances, while DWT's accuracy slightly declined under variable disturbances (99.70%). In contrast, SLT maintained 100% accuracy in both scenarios. Additionally, SLT consistently demonstrated superior processing efficiency, completing fault detection and classification in approximately 3.7 s, compared to 7.8 s for DWT. Mean squared error (MSE) values were comparable across methods, though DWT yielded marginally lower MSE under constant conditions. These quantitative results substantiate the earlier qualitative observations and further confirm that SLT offers a more balanced combination of high accuracy, low latency, and computational efficiency for real-time robotic fault detection applications.

A benchmark comparison with recent state-of-the-art methods further demonstrated the competitive performance of the proposed SLT-based framework. As shown in Table 10, while deep learning models such as CNN, LSTM, Transformer, and GNN-based frameworks achieved high diagnostic accuracy, their processing times exceeded 9 s, making them less suitable for fast-response real-time control applications. The SLT-MLP-ANN approach achieved the same 100% accuracy level in a fraction of the time (3.73 s), offering a practical and reliable solution for robotic fault diagnosis tasks. These results confirm that the proposed system not only maintains high diagnostic precision but also meets the real-time responsiveness demands of industrial robotic environments.

Future work

Although the proposed fault diagnosis framework demonstrated excellent performance in detecting simultaneous faults in robotic joints under variable load conditions, several opportunities exist to further enhance its capabilities. One of the primary areas for improvement lies in reducing the overall detection and classification latency, particularly to meet the stringent sub-10 millisecond response requirements of high-speed industrial control loops. Future research should focus on optimizing the computational efficiency of the SLT-MLP-ANN pipeline, potentially through algorithmic simplifications, hardware acceleration techniques, or embedded implementation on real-time microcontroller platforms. In addition, while this study employed time-frequency feature extraction methods, recent advancements in graph-based learning architectures have shown considerable promise for machinery fault diagnosis. Frameworks such as the Energy-Propagation Graph Neural Network (EG-SAGCN) and the Graph Causal Inference framework (GCI-ODG) have demonstrated superior performance in handling distributional shifts, modeling system interdependencies, and improving robustness in mechanical systems. Future work should explore integrating such graph neural network models into robotic joint fault detection systems, either as standalone classifiers or in hybrid architectures combining time-frequency and graph-based relational features. Moreover, extending the proposed framework to multi-robot collaborative systems and dynamic task environments would be valuable for industrial applications. This includes adapting the diagnostic system to manage continuously changing operational conditions, multiple degrees of freedom, and inter-robot interactions, where distributed or federated graph-based learning approaches could offer enhanced scalability and fault resilience. Finally, future investigations should also consider deploying the proposed system in diverse industrial settings, incorporating different robot models and joint configurations to further validate its generalizability and practical utility in real-world manufacturing and assembly processes.

Data availability

There is no additional supplementary material associated with this study, and any datasets used or analyzed are available from the corresponding author upon reasonable request.

Received: 3 May 2025; Accepted: 26 June 2025
Published online: 01 October 2025

References

1. Jaber, A. A. Design of an intelligent embedded system for condition monitoring of an industrial robot, Springer Thesis, Ph. D. Thesis Submitted to Newcastle University, (2017).
2. Terra, M. H. & Tinós, R. Fault detection and isolation in robotic manipulators via neural networks: A comparison among three architectures for residual analysis. *J. Robot. Syst.* **18** (7), 357–374 (2017).
3. Halme, J. Condition monitoring of a material handling industrial robot. In *Proc. 19th Int. Congress*. **IC'06**, 415–424 (2006). Lulea, Sweden.
4. Dumitru Baleanu *Wavelet Transform and some of its real-world Application* (InTech, 2015).
5. Daigle, M. J., Koutsoukos, X. D. & Biswas, G. Distributed diagnosis in formations of mobile robots. *IEEE Trans. Robot*. **23**(2), 353–369 (2007).
6. Liu, Y. & Jiang, J. Fault diagnosis method for mobile robots-using multi-CMAC neural networks. In *Proceedings of the IEEE International Conference on Automation and Logistics* 18–21, Jinan, China, pp. 903–907, (2007).
7. Huang, S. N. & Tan, K. K. Fault detection, isolation, and accommodation control in robotic systems. *IEEE Trans. Autom. Sci. Eng.*, **5**(3): 480–489 (2008).
8. Eski, I., Erkaya, S., Savas, S. & Yildirim, S. Fault detection on robot manipulators using artificial neural networks. *J. Robot. Comput.-Integr. Manuf.* **27** (1), 115–123 (2011).
9. Capisani, L. M., Ferrara, A. & de Loza, A. F. Fridman, manipulator fault diagnosis via higher order Sliding-Mode observers. *IEEE Trans. Industr. Electron.* **59** (10), 3979–3986 (2012).
10. Gómez-de-Gabriel, J. M., Mandow, A., Fernández-Lozano, J. & García-Cerezo, A. Mobile robot lab project to introduce engineering students to fault diagnosis in mechatronic systems. *IEEE Trans. Educ.* **58** (3), 187–193 (2015).
11. Jaber, A. A. & Bicker, R. Fault diagnosis of industrial robot bearings based on discrete wavelet transform and artificial neural network. *Int. J. Prognostics Health Manag.*, **7**(2), 13 (2016).
12. Zhou1, B., Qian, K. & Ma, X. Dai1, ellipsoidal bounding Set-Membership identification approach for robust fault diagnosis with application to mobile robots. *J. Syst. Eng. Electron.* **28** (5), 986–995 (2017).
13. Lin, C. & Boldbaatar, E. Fault accommodation control for a biped robot using a recurrent wavelet Elman neural network. *IEEE Syst. J.* **11** (4), 2882–2893 (2017).
14. Kamel, M. A., Yu, X. & Zhang, Y. Fault-Tolerant cooperative control design of multiple wheeled mobile robots. *IEEE Trans. Control Syst. Technol.* **26** (2), 756–764 (2018).
15. Monica, L. et al. A dynamic fault tolerance framework for remote robots. *IEEE Trans. Robot. Autom.*, **2**(4), 477–490 (1995).
16. EliahuKhalastchi, M. & Kalech fault detection and diagnosis in multi-robot systems: A survey. *Sensors* **19**(18), 4019 (2019).
17. Patton, R. J. & Lopez-Toribio, C. J. Soft computing approaches to fault diagnosis for dynamic systems: A survey, supervision and safety for technical processes. *Budapest Hung.* **33** (11), 303–315 (2000).
18. Schneider, H. & Frank, P. M. Observed based supervision and fault detection in robots using nonlinear and fuzzy logic residual evaluation. *IEEE Trans. Control Syst. Technol.* **4** (3), 274–282 (1996).
19. Crestani, D. Enhancing fault tolerance of autonomous mobile robots, robotics and autonomous systems. Elsevier, *68*, 140–155 (2015).
20. Andr´e, M. H. et al. *Differentially – Private Distributed Fault Diagnosis for Large – Scale Nonlinear Uncertain Systems, IFAC Papers OnLine* 51, 975–982 (Elsevier, 2018). 24.
21. VenkatVenkatasubramanian et al. A review of process fault detection and diagnosis part III: Process history based methods. *Comput. Chem. Eng.* **27** (3), 327–346 (2003).
22. Avizienis, A., Laprie, J. C., Randell, B. & Landwehr, C. Basic concepts and taxonomy of dependable and secure computing. *IEEE Trans. Depend. Secur. Comput.* **1** (1), 11–33 (2004).
23. Van Mien et al. Fault Estimation and accommodation for virtual sensor Bias fault in Image-Based visual servoing using particle filter. *IEEE Trans. Industr. Inf.* **14** (4), 1312–1322 (2018).
24. Alobaidy, M. A. A., Abdul-Jabbar, J. M. & Al-khayyt, S. Z. Slantlet transform used for faults diagnosis in robot arm. *Indones. J. Electr. Eng. Comput. Sci.* **25** (1), 281–290 (2022).
25. Alobaidy, A., Abdul-Jabbar, M. A., Jassim, D., Al-khayyt, S. Z. & M., & Faults diagnosis in robot systems: A review. *Al-Rafidain Eng. J. (AREJ)*. **25** (2), 164–175 (2021).
26. AlaaJaber, R. & Bicker Industrial Robot Fault Detection Based on Wavelet Transform and LabVIEW, First International Conference on Systems Informatics, Modelling and Simulations, School of Mechanical and System Engineering, Newcastle University, UK, (2014).
27. Theory Of Machines, (14th Edition) by, Khurmi, R. S. & Gupta, J. K. Khurmi Gupta Paperback, 1,071 Pages, Published 2015 by S.Chand & Company Ltd ISBN-13: 978-81-219-2524-2, ISBN: 81-219-2524-X.
28. Najm, M. I., Younis, A. D. & Majeed, F. A. Mathematical modelling and PID controller implementation to control linear and nonlinear quarter Car active suspension. *Al-Rafidain Eng. J. (AREJ)*. **28** (2), 113–121 (2023).
29. Majdi, H. S., Merzah, B. N., Al-Musawi, M. & Abdullah, A. R. S. T., Numerical simulation of heat transfer and flow enhancement through Multi-Row film holes for gas turbine blade cooling. *Math. Modelli. Eng. Probl.*, **10**(3). (2023).
30. Adaryani, M. R., Taher, S. A. & Guerrero, J. M. Improved direct model predictive control for variable magnitude variable frequency wave energy converter connected to constant power load. *J. Energy Storage*. **43**, 103175 (2021).
31. Wiranata, A., Mao, Z., Kuwajima, Y., Yamaguchi, Y., Muflikhun, M. A., Shigemune,H. & Maeda, S. Computer-controlled ultra high voltage amplifier for dielectric elastomer actuators. *Biomimetic Intell. Robot*. 100139 (2023).
32. Mamodiya, U. & Tiwari, N. Design and implementation of an intelligent single axis automatic solar tracking system. *Mater. Today Proc.* **81**, 1148–1151 (2023).
33. Vijayalakshmi, S. Robotic Car Using Arduino with Bluetooth Controller. (2019).
34. Shu, S., Wang, T., He, J., Chen, P., Xu, S., Li, C. & Tang, W. Bionic underwater multimodal sensor inspired by fish lateralis neuromasts. *Device* **1**(5) (2023).
35. Saeed, S. Z., Alobaidy, M. A. A. & Yosif, Z. M. Errors detection based on SDWT and BNN applied for position, velocity and acceleration signals of a wheeled mobile robot. *J. Rob. Control (JRC)*. **5** (5), 1291–1298 (2024).
36. Yosif, Z. M., Mahmood, B. S. & Saeed, S. Z. Artificial techniques based on neural network and fuzzy logic combination approach for avoiding dynamic Obstacles. *J.Européen Des. Systèmes Automatisés*, **55**(3). (2022).
37. Ashraf, E., Kabeel, A. E., Elmashad, Y., Ward, S. A. & Shaban, W. M. Predicting solar distiller productivity using an AI approach: Modified genetic algorithm with Multi-Layer perceptron. *Sol. Energy*. **263**, 111964. https://doi.org/10.1016/j.solener.2023.111964 (2023).
38. Mohapatra, P. et al. Artificial neural network-based prediction and optimization of centelloside content in Centella asiatica: A comparison between multilayer perceptron (MLP) and radial basis function (RBF) algorithms for soil and Climatic parameter. *S. Afr. J. Bot.* **160**, 571–585. https://doi.org/10.1016/j.sajb.2023.07.019 (2023).
39. Alobaidy, M. A. A., Yosif, Z. M., Alsoufi, M. S. & Al-Ashqar, S. Attendance system based on face recognition dependent on deep intelligent techniques. *Revue d'Intelligence Artificielle*. **38** (3), 1009 (2024).
40. Polenghi, A., Cattaneo, L. & Macchi, M. A framework for fault detection and diagnostics of articulated collaborative robots based on hybrid series modelling of artificial intelligence algorithms. *J. Intell. Manuf.* **35** (5), 1929–1947 (2024).
41. Alobaidy, M. A., Yosif, Z. M. & Alkababchi, A. M. Age-Dependent palm print recognition using convolutional neural network. *Revue d'Intelligence Artificielle*. **37** (3), 795. https://doi.org/10.18280/ria.370328 (2023).

42. Dehmamy, N., Barabási, A. L. & Yu, R. Understanding the representation power of graph neural networks in learning graph topology. *Adv. Neural. Inf. Process. Syst.*, **32**. (2019).
43. Chen, Z. et al. Graph neural network-based fault diagnosis: A review. (2021). arXiv:2111.08185.
44. Li, X. et al. *Energy-propagation Graph Neural Networks for Enhanced out-of-distribution Fault Analysis in Intelligent Construction Machinery Systems* (IEEE Internet of Things Journal, 2024).
45. Li, X. et al. Adaptive expert ensembles for fault diagnosis: A graph causal framework addressing distributional shifts. *Mech. Syst. Signal Process.* **234**, 112762 (2025).
46. Park, J. & Park, J. Physics-induced graph neural network: An application to wind-farm power Estimation. *Energy* **187**, 115883 (2019).
47. Perera, R., Guzzetti, D. & Agrawal, V. Graph neural networks for simulating crack coalescence and propagation in brittle materials. *Comput. Methods Appl. Mech. Eng.* **395**, 115021 (2022).
48. Liang, S. et al. EnGN: A high-throughput and energy-efficient accelerator for large graph neural networks. *IEEE Trans. Comput.* **70** (9), 1511–1525 (2020).
49. Zhang, X., Liu, J., Zhang, X. & Lu, Y. Self-supervised graph feature enhancement and scale attention for mechanical signal node-level representation and diagnosis. *Adv. Eng. Inform.* **65**, 103197 (2025).
50. Ding, M. H. T. & Han, T. SAGCN: Towards Structure-Aware Deep Graph Convolutional Networks on Node. In *Advances in Knowledge Discovery and Data Mining: 25th Pacific-Asia Conference, PAKDD 2021, Virtual Event, May 11–14, 2021, Proceedings, Part II* (Vol. 12713, p. 67). (Springer, 2021).
51. Sun, W., Ren, C., Xu, J. & Zhang, P. SAGCN: Using graph convolutional network with subgraph-aware for circRNA-drug sensitivity identification. *IEEE/ACM Trans. Comput. Biol. Bioinform.* (2024).
52. Wu, Q., Chen, Y., Yang, C. & Yan, J. Energy-based out-of-distribution detection for graph neural networks. ArXiv Preprint arXiv :230202914. (2023).
53. wang, D., Wei, Y. & shi, X. *Multi-Fault Identification of Rolling Bearings Using VMD and Optimized MCKD* (Engineering Research Ex, 2025).
54. Yue, K. et al. Physics-informed dual guidance method using physical envelope harmonic distribution and transfer learning for few-shot gear fault classification. *Eng. Appl. Artif. Intell.* **153**, 110956 (2025).
55. Li, X., Zhang, W., Xu, N. X. & Ding, Q. Deep learning-based machinery fault diagnostics with domain adaptation across sensors at different places. *IEEE Trans. Industr. Electron.* **67** (8), 6785–6794 (2019).
56. Zhang, W., Li, C., Peng, G., Chen, Y. & Zhang, Z. A deep convolutional neural network with new training methods for bearing fault diagnosis under noisy environment and different working load. *Mech. Syst. Signal Process.* **100**, 439–453 (2018).
57. Zhao, R. et al. Deep learning and its applications to machine health monitoring. *Mech. Syst. Signal Process.* **115**, 213–237 (2019).
58. Gawde, S. et al. Multi-fault diagnosis of industrial rotating machines using Data-driven approach: A review of two decades of research. *Eng. Appl. Artif. Intell.* **123**, 106139 (2023).
59. Wang, R., Dong, E., Cheng, Z., Liu, Z. & Jia, X. Transformer-based intelligent fault diagnosis methods of mechanical equipment: A survey. *Open. Phys.* **22** (1), 20240015 (2024).
60. Yang, B., Lei, Y., Jia, F. & Xing, S. An intelligent fault diagnosis approach based on transfer learning from laboratory bearings to locomotive bearings. *Mech. Syst. Signal Process.* **122**, 692–706 (2019).
61. Widodo, A. & Yang, B. S. Support vector machine in machine condition monitoring and fault diagnosis. *Mech. Syst. Signal Process.* **21** (6), 2560–2574 (2007).
62. Li, X. et al. Energy-propagation graph neural networks for enhanced out-of-distribution fault analysis in intelligent construction machinery systems. *IEEE Internet Things J.* (2024).
63. Ren, J. & Teoh, S. S. A hybrid adaptive fusion deep learning model for fault diagnosis of rotating machinery under noisy conditions. *IEEE Access* (2025).
64. Li, X., Li, M., Liu, B., Lv, S. & Liu, C. A novel transformer network based on Cross–Spatial learning and deformable attention for composite fault diagnosis of agricultural machinery bearings. *Agriculture* **14** (8), 1397 (2024).

Acknowledgements

The authors would like to thank the editorial and review committees for the upcoming review and for the valuable time that will be devoted to the review. The authors wish to thank the staff of the College of Engineering - University of Mosul for their support.

Author contributions

Muhamad Azhar Abdilatef Alobaidy contributed to the conceptualization, methodology, investigation, and preparation of the original draft. Jassim M. Abdul-Jabbar was responsible for data curation, software development, formal analysis, and validation. Mohammed Aly provided supervision, project administration, funding acquisition, and contributed to writing, reviewing, and editing the manuscript. Reza Hassanpour contributed to visualization, resource provision, validation, and writing, reviewing, and editing the manuscript.

Funding

Open access funding provided by The Science, Technology & Innovation Funding Authority (STDF) in cooperation with The Egyptian Knowledge Bank (EKB).

Declarations

Competing interests

The authors declare no competing interests.

Additional information

Correspondence and requests for materials should be addressed to M.A.